



ELSEVIER

Contents lists available at ScienceDirect

Journal of Fluids and Structures

journal homepage: www.elsevier.com/locate/jfs

Nonlinear single-mode and multi-mode panel flutter oscillations at low supersonic speeds



Anastasia Shishaeva^{a,b}, Vasily Vedenev^{a,*}, Andrey Aksenov^b

^a Lomonosov Moscow State University, 1, Leninskie Gory, Moscow, Russia

^b Tesis LTD, 18, Yunnatov str., Moscow, Russia

ARTICLE INFO

Article history:

Received 10 November 2014

Accepted 16 May 2015

Keywords:

Panel flutter

Single mode flutter

Single degree of freedom flutter

Internal resonance

Nonlinear oscillations

Chaotic oscillations

ABSTRACT

In this study we numerically analyse nonlinear flutter oscillations of elastic plate in a gas flow. In contrast to many other studies, we use inviscid flow model instead of piston theory or other simplified aerodynamic theories. This study aims to investigate the region of low supersonic Mach numbers, $1 < M < 2$, where several plate eigenmodes can be simultaneously unstable, and resulting oscillations are governed by nonlinear interaction of growing modes. Three types of unstable plate behaviour have been obtained. First, at $0.76 < M < 1$, the plate diverges. Second, at $1 < M \leq 1.67$, single-mode flutter occurs in three distinct forms: limit cycle in the first mode ($1 < M < 1.33$ and $1.5 < M \leq 1.67$) or higher modes; limit cycle in the first and second modes being in internal 1:2 resonance ($1.12 < M < 1.33$ and $1.42 < M < 1.5$); and non-periodic oscillations with several dominating frequencies being in more complex ratio ($1.33 < M < 1.42$). Third, at $M = 1.82$ and increased dynamic pressure, coupled-mode flutter appears. Amplitudes and spectra of each limit cycle type are analysed. The role of aerodynamic nonlinearity in the formation of limit cycle oscillations is discussed.

© 2015 Elsevier Ltd. All rights reserved.

1. Introduction

Aeroelastic instability of plates in a gas flow has been investigated in numerous studies in the context of the panel flutter problem (Movchan, 1957; Bolotin, 1963; Grigolyuk et al., 1965; Dugundji, 1966; Dowell, 1974; Mei et al., 1999). In the case of subsonic flow, the primary instability type is static divergence, whereas in supersonic flow, instability has an oscillatory nature, i.e., the plate flutters. Flutter instability, in turn, can be either coupled- or single-mode flutter. The first one occurs because of coalescence of the plate eigenfrequencies caused by the action of the flow; it has been studied in detail in the 1950s to 1970s using aerodynamic piston theory. The other flutter type, single-mode flutter, occurs at lower Mach numbers, $1 < M < 2$. Recently, detailed investigation of linear single-mode flutter boundaries has been conducted (Vedenev, 2005, 2012, 2013a); also, this flutter type has been observed in experiments by Vedenev et al. (2010). The unusual result that has been obtained is that there is a range of Mach numbers and plate lengths where several plate eigenmodes are simultaneously unstable. Hence, the development of initial perturbation consisting of those modes and formation of the limit cycle is governed by nonlinear interaction of the unstable eigenmodes.

* Corresponding author. Tel.: +7 9163382382.

E-mail addresses: nsh@tesis.com.ru (A. Shishaeva), vasily@vedeneev.ru (V. Vedenev), andrey@tesis.com.ru (A. Aksenov).

URL: <http://www.vedeneev.ru> (V. Vedenev).

In this study, aeroelastic instability of a plate in an airflow is investigated by direct time-domain numerical simulation. Plate and gas flow motions are modelled in solid and fluid codes, respectively, with direct coupling between them. The effect of the boundary layer over the plate is neglected. The main goal of this study is to investigate the nonlinear development of growing oscillations in case of several linearly growing eigenmodes.

Several time-domain simulations of nonlinear panel flutter were performed at conditions of transonic and low supersonic speeds by different authors (Bendiksen and Davis, 1995; Gordnier and Visbal, 2002; Hashimoto et al., 2009; Alder, 2015). Their studies showed that limit cycle oscillations resulting from single-mode linear growth mechanism occur in the form of travelling wave with dominating first-mode shape. In the present study, we show that there is a range of Mach numbers where such a limit cycle is not unique, and the other limit cycle includes two first modes being in 1:2 internal resonance. For higher Mach numbers, where higher eigenmodes become unstable, high-frequency limit cycles and non-periodic oscillations occur. Such high-frequency oscillations, occurring on an aircraft panel, yield much faster fatigue damage than the first-mode limit cycle or conventional coupled-mode flutter oscillations.

In contrast to other panel flutter studies, we consider two problem formulations: air flowing over one side of the panel and over two sides with twice lower air density. When linearising, these formulations become identical, such that the difference in the nonlinear problem represents the effect of aerodynamic nonlinearity. We show that in all cases, except a very narrow vicinity of $M=1$, the results obtained from both formulations are similar, i.e., all limit cycle oscillations observed are caused by structural nonlinearity only, whereas the aerodynamic nonlinearity is negligible.

2. Formulation of the problem

We investigate two-dimensional motion of an elastic plate in a uniform airflow. The air flows over one or two sides of the plate. In the first case, the pressure underneath the plate equals the free-stream pressure; in the latter case, the flow parameters along both sides of the plate are equal. The unperturbed state of the plate is flat.

The flow over one side of the plate represents the classical panel flutter model. The two-sided flow is studied to reveal the role of aerodynamic nonlinearity in limit cycle oscillations, as will be discussed below.

2.1. Plate model

The elastic plate of length $L_p=0.3$ m and thickness $h_p=0.001$ m is clamped at both edges ($w(x, t) = \partial w(x, t)/\partial x = 0$), where it smoothly passes into a rigid surface (Fig. 1). The plate is made of steel with Young's modulus $E = 2 \times 10^{11}$ Pa, Poisson's coefficient $\nu = 0.3$, and density $\rho_m = 7800$ kg/m³. In dimensionless terms, the plate stiffness and length are

$$D = \frac{D_p}{a^2 \rho_m h^3} = 21.4, \quad L = \frac{L_p}{h_p} = 300, \quad (1)$$

where $D_p = Eh^3/(12(1-\nu^2))$ is the dimensional plate stiffness, and $a=331$ m/s is the speed of sound in the air. Similar values of dimensionless parameters correspond to other metal materials (e.g., aluminium and titanium). The plate is governed by the nonlinear Mindlin plate model, where elastic strains are calculated through Koiter–Sanders shell theory.

During a short initial time range $t = 0 \dots \varepsilon$, where $\varepsilon = 0.0002$ s, a slight disturbing force is applied to the panel to introduce initial perturbation of the system. At $t > \varepsilon$, no external force is applied to the plate and the flow so that the subsequent behaviour of the system is governed by the fluid–structure interaction only.

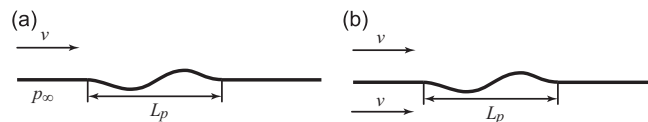


Fig. 1. Plate in a gas flow: one-sided (a), two-sided (b) flow.

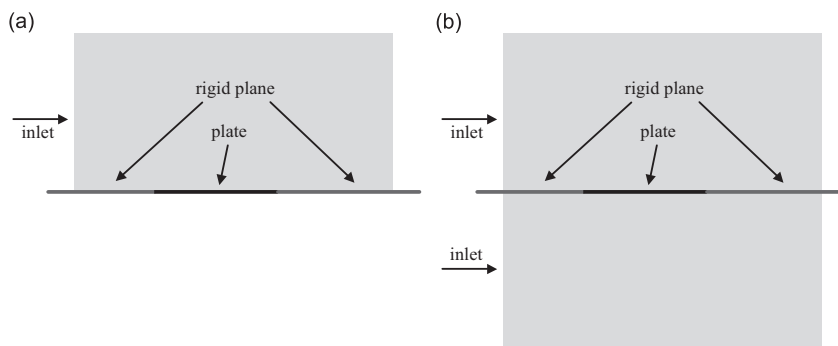


Fig. 2. Simulation domain: one-sided (a), two-sided (b) flow.

2.2. Aerodynamic model

The simulation domain of the gas flow is a rectangular 0.6×0.3 m (one-sided flow) or a square 0.6×0.6 m (two-sided flow), as shown in Fig. 2. We consider inviscid perfect gas with air properties assigned. To deal with more robust numerical solutions, we assign a small flow viscosity, i.e., the flow is governed by Navier–Stokes equations. In order to neglect any shear layer occurring in a viscous flow over rigid boundaries, and any turbulence-related issues, we apply a special boundary condition along the plate surface, that is, instead of the classical no-slip condition, we apply the free-slip condition:

$$v_n = v_p, \quad \partial v_\tau / \partial n = 0,$$

where v_n and v_τ are normal and tangent velocity components of the flow, respectively, and v_p is the plate vertical velocity. This way we avoid the formation of the boundary layer and do not need to excessively refine the mesh near the plate. Based on our observations, the viscosity specified is small enough to not affect the flow and the plate oscillations. Thus, this formulation is equivalent to simulating the flow of inviscid fluid, whereas the viscosity is needed only for numerical stabilisation and does not influence the solution.

Other boundary conditions for the flow depend on whether flow is subsonic or supersonic. For supersonic flow speeds, we assign the following conditions:

- Inlet: Constant velocity, pressure, and temperature. The same parameters are specified over the simulation domain at $t=0$ as initial conditions. Temperature at inlet is equal to 273 K in all cases studied. Two other flow parameters, namely, flow speed and pressure, are varied. Hereafter we will use two dimensionless parameters that represent flow condition: Mach number and flow density

$$M = \frac{v}{a}, \quad \mu = N \frac{\rho}{\rho_m}, \quad (2)$$

where ρ is the dimensional flow density, and $N=1$ and 2 represent the case of one- and two-sided flows, respectively. This definition of μ provides comparable total unsteady pressure force acting on the plate when one- and two-sided flows are considered. Given that the temperature is fixed, the Mach number is governed only by the inlet velocity, whereas μ is governed only by the inlet pressure. Dimensionless dynamic pressure and mass ratio commonly used in panel flutter studies can be expressed through M and μ as follows:

$$\lambda^* = \frac{\rho v^2 L_p^3}{D_p} = \frac{L^3}{D^3} \mu M^2 = 1.26 \cdot 10^6 \cdot \mu M^2, \quad \mu^* = \frac{\rho L_p}{\rho_m h_p} = L \mu = 300 \cdot \mu.$$

- Top, bottom, and aft domain boundaries: The condition of free flow outlet is assigned. The values of the velocity, pressure, and temperature at the boundary cells are equal to those at the next layer of the cells normal to the boundary. For the aft boundary, this condition defines the flow parameters at the boundary cells but does not affect the flow inside the domain because the flow is supersonic. For top and bottom boundaries, this condition provides no reflection of incident waves so that these boundaries do not affect the plate.

For subsonic flow speeds, another set of boundary conditions is used:

- Inlet: Total pressure and temperature of the flow are assigned. As well as for the supersonic case, the temperature is always equal to 273 K.
- Top, bottom, and aft domain boundaries: The flow pressure is specified.

In all subsonic cases, we ensured that the inlet pressure obtained in analysis coincides with the pressure defined at other boundaries, such that the inlet velocity also takes the desired value. Note that in subsonic case the boundary conditions are not non-reflecting. However, we ensured that they are located far enough from the plate and do not affect it (see Section 6.1 below).

Let us consider the difference between one-sided and two-sided flows. If the flow equations are linearised, both cases would be equivalent. Indeed, when the plate bends upwards, the top- and bottom-side flows produce the same unsteady pressure but with opposite signs. Considering that plate normal directions are also opposite, both flows produce the same net pressure as a one-sided flow with double density would (that is why N is present in (2)). However, in the nonlinear problem, these formulations are unequal. When the plate bends upwards, the top-side flow has a shock wave followed by an expansion fan, whereas the bottom-side flow has an expansion fan followed by a shock wave, which is, clearly, not the same in nonlinear case. Thus, the difference between one- and two-sided flows is produced only by the aerodynamic nonlinearity.

3. Numerical technique

Analysis is conducted by using two coupled commercial codes. Plate motion is simulated in Abaqus, a finite-element code originally developed for stress analysis. The flow is simulated in a finite-volume code FlowVision developed by Tesis LTD for aero/hydrodynamic applications.

Interaction between the codes is organised through direct coupling mechanism along the surface of the deformed plate (Aksenov et al., 1998, 2008). Both codes are executed in turns; exchanges occur at each time step according to conventional

serial staggered (CSS) procedure (Fig. 3). The displacements and velocities of the plate points are sent from Abaqus to FlowVision, whereas the pressure distribution along the plate surface is sent back from FlowVision to Abaqus.

Mesh properties used in the simulation are as follows. The Abaqus plate model consists of hexahedral finite elements, with 60 elements along the chordwise direction. The FlowVision flow model consists of 50×772 (length \times height) finite volumes for the

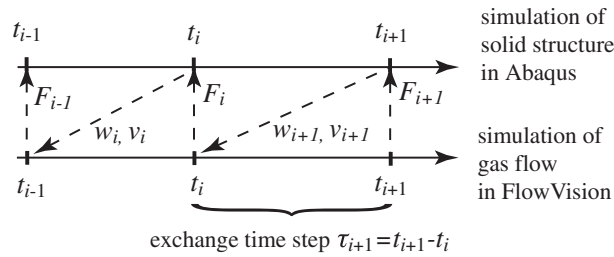


Fig. 3. Exchange algorithm between FlowVision and Abaqus.

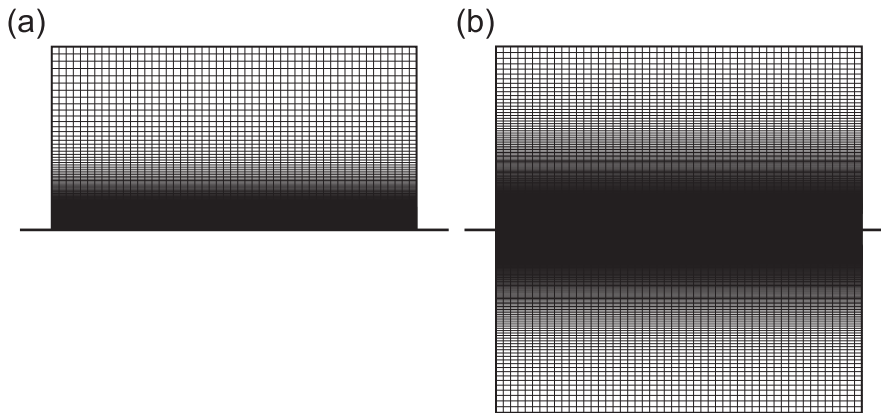


Fig. 4. Mesh of the flow domain: one-sided (a), two-sided (b) flow.

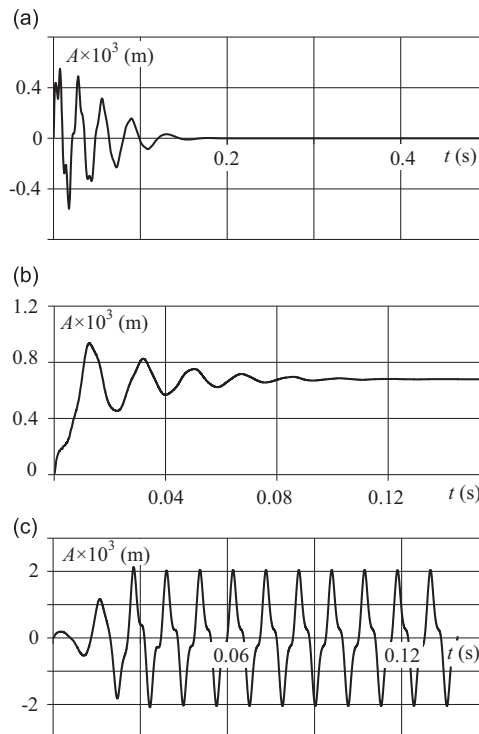


Fig. 5. Deflection of the reference point vs. time: stability ($M=0.7$, a), divergence ($M=0.9$, b), flutter ($M=1.06$, c).

two-sided flow and 50×494 for the one-sided flow (Fig. 4). The vertical size of finite volumes varies from 0.0001 m near the plate to 0.01 m in the far field of the simulation domain. A special mesh convergence study was performed (the results are presented in the next section), which shows that the mesh is fine enough to obtain an accurate limit cycle solution. When solving the problem with moving boundary, FlowVision uses a subgrid resolution technique (Aksenov et al., 1998) to capture the plate motion.

Both Abaqus and FlowVision solvers use implicit time integration schemes. The initial time step is 0.0001 s. During the analysis, the adaptive time step equal for both solvers is calculated through maximum convective ($= 10$) and surface ($= 1$) Courant numbers by the FlowVision solver.

It is convenient to analyse plate behaviour by watching deflection A of a reference point plotted versus time. The reference point is located at 0.22 m downstream of the leading edge of the elastic plate, which is approximately $3/4$ of the plate length. Fourier analysis is used to calculate the spectra of limit cycles observed.

Three types of the plate behaviour were observed at various flow conditions: stability, divergence, and flutter. In the case of stability, the perturbed plate oscillates with rapidly decreasing amplitude and returns to the initial position. The reference point behaviour is plotted in Fig. 5a. In the case of divergence (which was detected only for $M < 1$), the plate is stabilised in a deflected position (Fig. 5b). In the case of flutter (which was observed only for $M \geq 1$), the plate oscillation amplitude increases and then stabilises at a nonzero value; the plate oscillates in a limit cycle (Fig. 5c).

In most cases, one- and two-sided flows provide the same divergent states or flutter oscillations. The only difference is seen at transonic speeds, as discussed below. In other cases, the results coincide so that we do not present them separately.

4. Convergence study

To ensure the numerical adequacy of the model, we conducted a series of test simulations under the same physical parameters and different grid sizes and time steps. We also checked the influence of the disturbing force amplitude in order

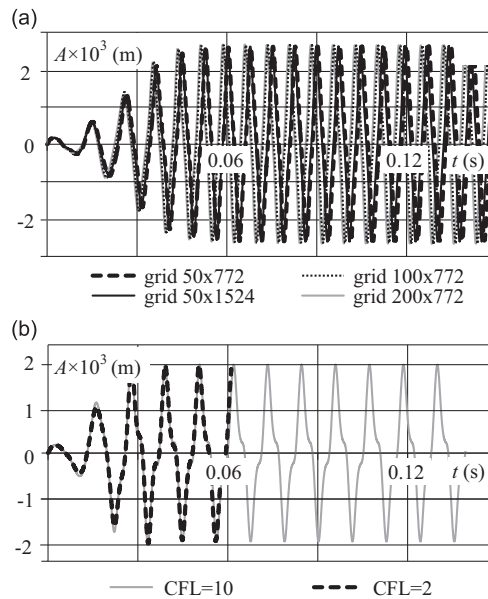


Fig. 6. Reference point deflection obtained on different grids for $M=1.12$, $\mu = 1.64 \cdot 10^{-4}$ (a); deflection obtained with different time steps for $M=1.06$, $\mu = 1.64 \cdot 10^{-4}$ (b).

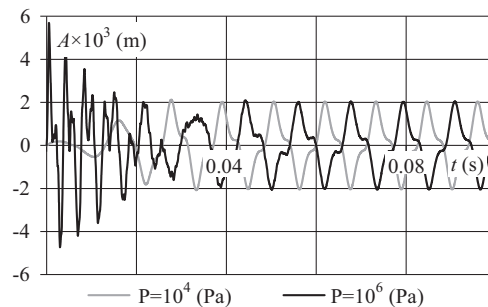


Fig. 7. Reference point deflection in time for different perturbation load, $M=1.06$, $\mu = 1.64 \cdot 10^{-4}$.

to make sure that the oscillations occur because of fluid–structure interaction and not because of numerical inaccuracies.

Fig. 6a shows the simulation results obtained on different grid sizes of the flow domain. It is seen that the limit cycle is the same in all cases. A small phase shift occurs because of a slight difference in the transient phase of the oscillation growth. Given that the limit cycles are almost identical, we conclude that the convergence in grid size is achieved.

Fig. 6b shows the simulations with two time steps. They correspond to Courant numbers (CFL) 2 and 10. The results are similar, which means that the convergence in time step is also achieved.

Fig. 7 shows the plate oscillations for different amplitudes of the initial disturbance. Despite different initial phases of the limit cycle formation, caused by different disturbance amplitudes, in both cases the resulting limit cycle is the same. This result proves that the numerical model is adequate, and the limit cycle oscillations are caused by physical fluid–structure interaction.

The results shown in Figs. 6 and 7 represent the case of relatively small Mach numbers, when the limit cycle is unique. For higher Mach numbers, when two or more stable limit cycles exist (see below), the results with different time steps and

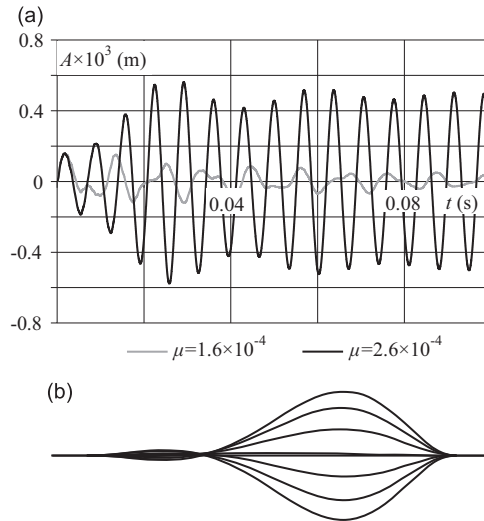


Fig. 8. Deflection of the reference point (a), oscillation mode shape (b) in case of coupled-mode flutter.

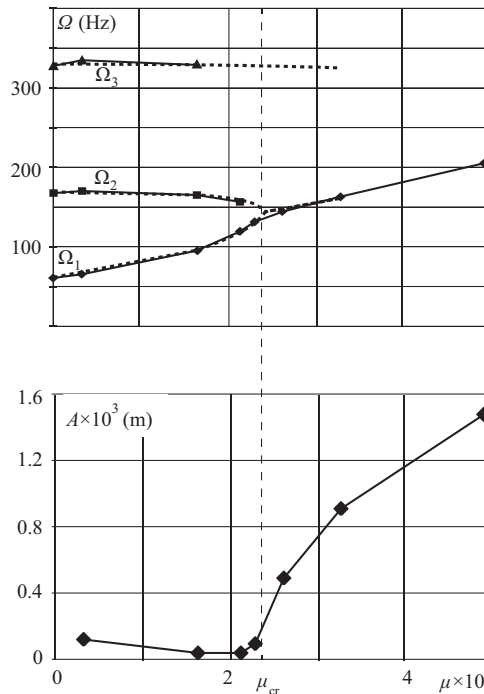


Fig. 9. The first three eigenfrequencies (top), oscillation amplitude (bottom) for $M = 1.82$. Results of the present study (continuous) and of Vedenev, 2013a (dotted).

mesh sizes differ from each other. First, the transient behaviour preceding the limit cycle is different and can be very long, up to hundreds of resulting limit cycle periods. Second, the established limit cycle can differ because there are more than one possible limit cycles. We consider this behaviour natural because the transient process is somewhat unstable, and the only important matter is the final limit cycle. In the case of two limit cycles, we checked that oscillations always fall into one of them, regardless of the preceding transient behaviour. In the case of high-frequency non-periodic oscillations, we compared the spectra obtained with different numerical parameters and made sure that they are similar.

5. High Mach numbers: observation of the coupled-mode flutter

We start the survey of the results obtained from the coupled-mode flutter. We set the Mach number $M=1.82$ and vary the dimensionless flow density μ in the range $3 \cdot 10^{-5} \leq \mu \leq 5 \cdot 10^{-4}$. These parameter values are chosen such that piston theory is still valid, and according to Movchan (1957), the coupled-mode flutter should occur. The spectrum of the limit cycle should consist of one frequency located between the first and second natural frequencies of the plate; to make sure that at least two first modes are excited, the initial perturbation load contained both first- and second-mode shape components.

The following results are obtained. When μ is not too large, the plate oscillates with a small amplitude decreasing in time (Fig. 8a). The spectrum mostly consists of two frequencies, corresponding to the first two modes. When μ increases, the first frequency increases, whereas the second decreases, as shown in Fig. 9a. In this figure, the results of the linear eigenfrequency calculation (Vedenev, 2013a) are also plotted for comparison; the difference is negligible. At $\mu = \mu_{cr}$, the first and the second frequencies coalesce so that for $\mu > \mu_{cr}$ only one frequency is detected in the oscillation spectrum. Coalescence is accompanied by the appearance of a limit cycle, whose amplitude increases with increase of μ (Fig. 9b). The oscillation mode shape is shown in Fig. 8b. It looks like a mixture of the first and second natural plate modes: it has a node located at approximately 1/4 plate length from the leading edge, whereas the amplitude of the rear part of the plate is much higher than that of the front part.

The critical dimensionless flow density (i.e., flutter boundary) obtained in our simulation is $\mu_{cr} = 2.39 \cdot 10^{-4}$. The theory based on piston theory (Grigolyuk et al., 1965) provides the following criterion of the coupled-mode flutter:

$$\frac{M^2}{\sqrt{M^2-1}} > \frac{D_p}{a^2 \rho L_p^3} \chi_{cr} = \frac{D}{\mu L^3} \chi_{cr}. \quad (3)$$

The value of χ_{cr} depends on boundary conditions, for the plate clamped at both edges $\chi_{cr} = 636$ (Grigolyuk et al., 1965). The substitution of $M=1.82$ and plate parameters (1) into (3) yields $\mu_{cr} = 2.31 \cdot 10^{-4}$. This value is in 3% discrepancy with the value obtained in this study.

Therefore, we conclude that the coupled-mode flutter boundary is correctly captured by our simulation. The overall coupled-mode flutter properties, such as coalescence of eigenfrequencies and limit cycle mode shape, are correctly simulated. This result provides additional verification of the model, and we can now proceed to the results obtained for lower Mach numbers, which are the primary interest of this work.

6. Subsonic and low supersonic Mach numbers: observation of the panel divergence and single-mode flutter

To analyse the plate behaviour at subsonic, transonic, and low supersonic Mach numbers, we fixed $\mu = 1.64 \cdot 10^{-4}$ and varied M from 0.7 to 2.0. This value of μ is small enough, comparing with μ_{cr} from the previous section, to avoid any coalescence of eigenfrequencies, and, hence, to avoid the coupled-mode flutter.

6.1. Subsonic speeds

For the parameters chosen, the plate is stable for $M \leq 0.76$. At $M > 0.76$, the perturbed plate is stabilised at a deformed state so that the deflection of the reference point tends to a constant value as $t \rightarrow \infty$ (Fig. 10a). The shape of the diverged

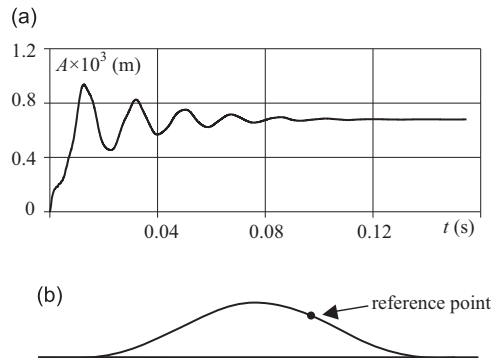


Fig. 10. Reference point deflection in time (a), plate shape (b) at divergence. $M=0.909$.

plate is close to the first natural mode shape (Fig. 10b). With the increase of M , the maximum plate amplitude increases, whereas the diverged shape slightly changes: the maximum deflected position shifts a little downstream. The Mach number distribution around the diverged plate is shown in Fig. 11. The figure shows that the flow along all domain boundaries is undisturbed. This means that even if the boundary conditions are not non-reflecting in the subsonic case, the boundaries are located far enough from the plate and do not affect the diverged state.

The divergence of the plate at subsonic speeds is consistent with the general plate behaviour studied by Dowell (1974). In our analysis, there is no difference in the plate shape when the air flows over one or both sides of the plate; in particular, upwards and downwards divergence amplitudes coincide. This result agrees with the study of Gordnier and Visbal (2002), who also showed that for essentially larger dynamic pressure than considered here, the downwards divergence amplitude becomes larger than the upwards divergence amplitude.

6.2. Transonic speeds

Mach numbers $M \approx 1$ correspond to a borderline state between divergence and single-mode flutter. Consider the two-sided flow. The plate oscillates (Fig. 12a), but the dominant frequency, 24 Hz, is less than half the first natural frequency of

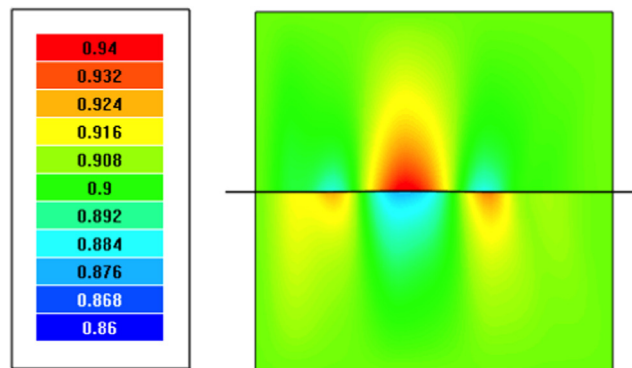


Fig. 11. Mach number distribution for the static plate deflection at $M=0.909$.

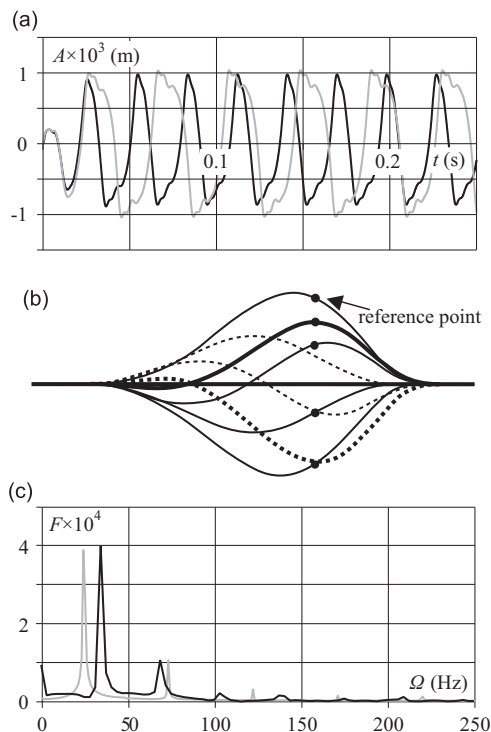


Fig. 12. Reference point deflection in time (a), instantaneous plate shapes (continuous and dashed curves represent motion down and up, respectively; bold curves represent the plate shape in delayed positions) (b), spectrum (c) at $M=1.0$. One-sided flow (black lines), two-sided flow (grey lines).

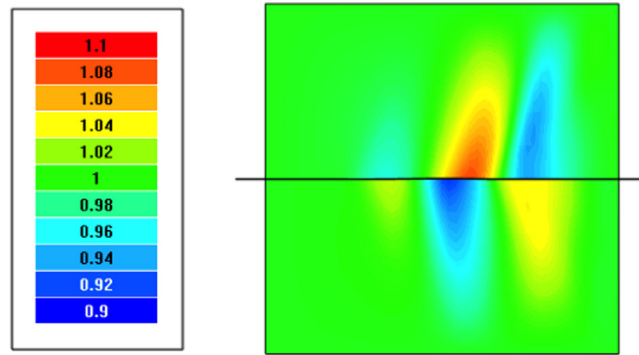


Fig. 13. Snapshot of the Mach number distribution for the maximum plate deflection at $M=1.0$.

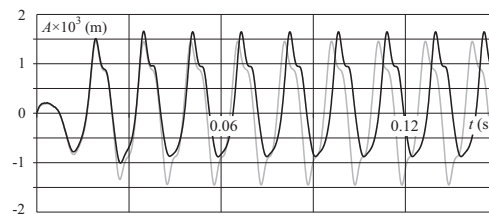


Fig. 14. Reference point deflection at $M=1.01$. One-sided flow (black line), two-sided flow (grey line).

the plate (Fig. 12c). In contrast to oscillations that occur at higher M , the plate motion is delayed in positions close to maximum and minimum deflections. Such oscillations can be represented as follows. The plate diverges upwards and stays in this position for some time. This delay can be considered as local stability of the diverged state of small duration. However, the aerodynamic pressure at $M \approx 1$ can no longer support the plate in the static position, and the plate buckles to the opposite diverged state. As a result, the oscillations are far from harmonic; in fact, they consist of opposite divergence states changing each other. Note that in contrast to subsonic divergence, the plate shapes in the delayed positions (shown by bold curves in Fig. 12b) are not purely first-mode shape, but have a clearly visible second-mode component. The oscillation mode shape has a form of a travelling wave (Fig. 12b), exactly as predicted by Bendiksen and Davis (1995). The distribution of Mach number along the flow domain is shown in Fig. 13; a significant change from the case of $M < 1$ is observed.

For transonic flow, the discrepancy between one- and two-sided flows is clearly visible in Fig. 12. While the oscillations in the two-sided flow are symmetrical, i.e., bends upwards and downwards are similar, in the one-sided flow the symmetry disappears: though delays are similar in the downwards bend positions, there is almost no delay in the upper position (Fig. 12a). As a result, the oscillation frequency is slightly higher in the one-sided flow (34 Hz), but still about half the first natural frequency. The difference between one- and two-sided flows is explained by different nonlinearities in shock waves and expansion fans appearing when the plate bends up or down. At slightly larger M , this non-symmetry becomes more pronounced, as shown in Fig. 14 for $M=1.01$.

Note that the time series in Fig. 12a is qualitatively similar to those obtained by Bendiksen and Davis (1995), Gordnier and Visbal (2002), and Alder (2015). The discrepancy in the amplitude is caused by different flow conditions and plate lengths used in those studies.

6.3. Supersonic speeds: non-resonant limit cycle oscillations

We now proceed to the case of $M > 1$. Note that the smallness of the flow density excludes the possibility of a coupled-mode flutter. Therefore, all oscillations that will be observed hereunder are caused by the single-mode flutter mechanism and the nonlinear mode interaction.

With the increase of M , the oscillation frequency rapidly increases, transonic-type delays disappear, so that at $M=1.05$, the limit cycle oscillations become symmetrical, and any discrepancy between one- and two-sided flows disappears.

In the range of Mach numbers $1.05 \leq M \leq 1.12$, we observed pure single-mode flutter oscillations (Figs. 15 and 16). The plate shape is close to the first natural mode shape; the deflections of the plate upwards and downwards are symmetrical to each other. Oscillations have a certain component of travelling wave moving downstream; however, the higher the Mach number, the more standing the oscillation. The spectrum of the reference point oscillations consists of two peaks being in ratio 1:3. The second peak is caused by a cubic nonlinearity of the plate and is not associated with a separate eigenmode.

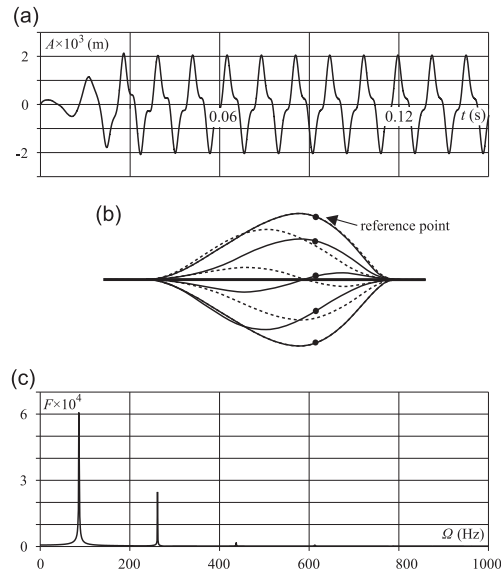


Fig. 15. Reference point deflection in time (a), plate shape (continuous and dashed curves represent motion down and up, respectively) (b), spectrum (c) at single-mode flutter. $M=1.06$.

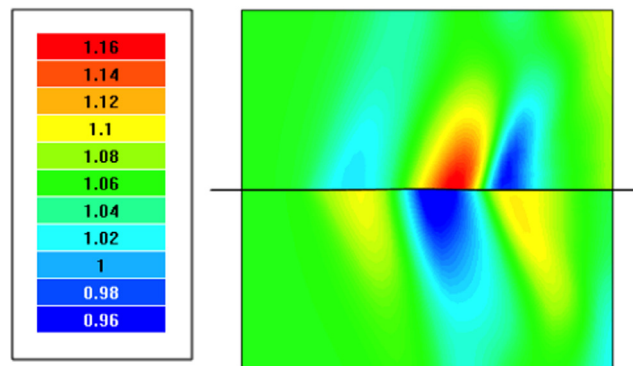


Fig. 16. Snapshot of the Mach number distribution for the maximum plate deflection at $M=1.06$.

6.4. Supersonic speeds: resonant limit cycle oscillations

In the range $1.12 < M < 1.33$, the limit cycle oscillations are unsymmetrical (Figs. 17 and 18). During the initial phase of the oscillation growth, the plate oscillates symmetrically, and the mode shape is the same as in Fig. 15b. Starting from a moment when the nonsymmetry appears, the growth of the second natural mode is clearly seen in the oscillation shape (Fig. 17b). Oscillations have a travelling wave component, but in contrast to the case of the non-resonant limit cycle, its direction is changed from downstream to upstream when the direction of the plate motion is changed from upwards to downwards. In other words, the plate shape passes the same states when the plate moves upwards and downwards, but in reverse orders. Compared with the non-resonant limit cycle, one more peak appears in the oscillation spectrum, which is in 1:2 ratio with the frequency of the first peak (Fig. 17c). We conclude that the growth of the second natural mode and nonsymmetry of oscillations is caused by internal 1:2 resonance between the first and the second modes.

Note that the possibility of a limit cycle that includes internal 1:2 resonance was analytically proved by Vedenev (2013b). Its mechanism consists of the following steps, clearly seen in the present simulations:

1. Because of linear instability, the first mode starts to grow. Oscillations are symmetrical, as only one mode is present yet.
2. As the system is nonlinear, the oscillation frequency also grows, following the amplitude. For the clamped plate, ratio of the first and second natural frequencies is less than 1/2. While the first mode grows, the ratio of the first to the second frequency of nonlinear oscillations also grows and at some moment equals 1/2.
3. Starting from this moment, the second mode is excited because of internal resonance. The most impressive feature is that the second mode is still linearly stable (i.e., damped), and its growth is maintained only by the resonance with the first mode that, in turn, is maintained by the aeroelastic instability.

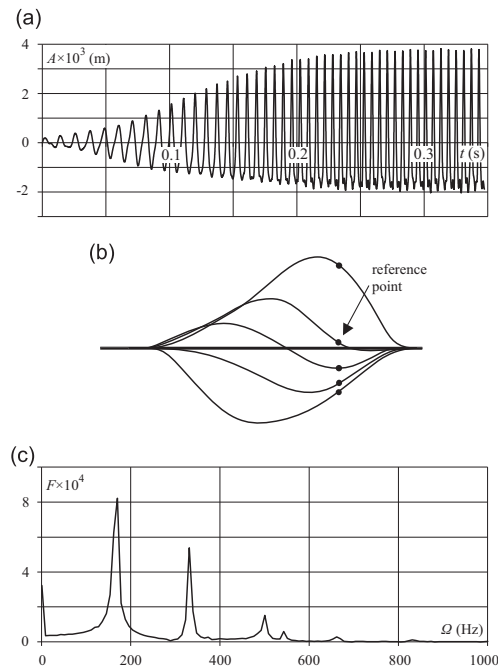


Fig. 17. Example of the reference point deflection in time (a), plate shape (b), and spectrum (c) at the flutter with internal resonance. $M=1.3$.

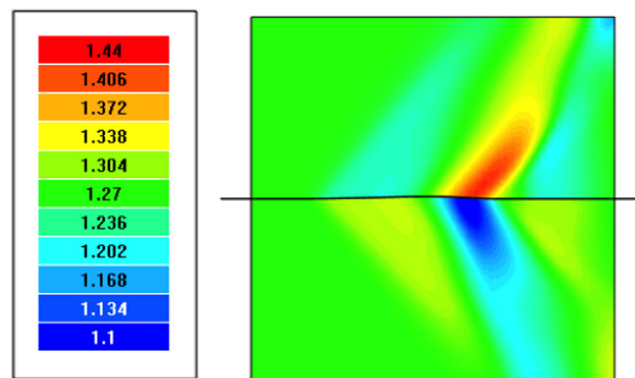


Fig. 18. Snapshot of the Mach number distribution for the maximum plate deflection at $M=1.27$.

- Growth of the first and second modes occurs until the following energy balance is established. The energy transfers from the flow to the first mode because of the instability of the latter. Next, this energy transfers to the second mode through nonlinear coupling between two modes. Finally, the same amount of energy transfers from the second mode to the flow because this mode is linearly damped. When this balance is achieved, the amplitudes of both modes reach their stable values, and the plate oscillates in a limit cycle.

The key step in the formation of the resonant limit cycle is step 3, when frequencies of nonlinear oscillations in the first and the second modes are in exact ratio 1:2 (Vedeneev, 2013b). If this moment is somehow passed without exciting the second mode, the non-resonant limit cycle should continue without any changes. Thus, based on the mechanism described, there should be coexistence of two limit cycles: resonant and non-resonant. Evasion of step 3 can be organised, for example, by applying an initial disturbing force that, first, has no second-mode component in the spatial distribution along the plate, and, second, has a sufficiently high amplitude, such that the initial nonlinear oscillation in the first mode has a frequency that is more than half the nonlinear frequency of the second mode. In such a case, step 3 will be immediately passed without exciting the second mode.

Let us consider results obtained with such a high-amplitude exciting force. First, for Mach number $M < M_{res}$, where $M_{res} \approx 1.13$ is the Mach number at which the resonant limit cycle appears, the increase of the force does not change the resulting limit cycle because this cycle is unique. The reason is that the stabilisation of the resonant limit cycle amplitude described in step 4 cannot be achieved for $M < M_{res}$: the plate energy will flow out to the air (Vedeneev, 2013b). Such a calculation is shown in Fig. 7 for $M=1.06$. Next, for M slightly higher than M_{res} , both resonant and non-resonant limit cycles are close to each other, and a very slight disturbance can switch the oscillation from one limit cycle to the other. Fig. 19 shows the

oscillations of the plate caused by three different exciting forces. The first force, pressure $P = 10^4$ Pa, consists of both first and second spatial mode components. It yields the resonant limit cycle based on the above-mentioned mechanism. The second force, $P = 10^6$ Pa, with exactly the same spatial distribution, yields the same limit cycle, though steps 1–3 in the evolution of the oscillations are missed: the same limit cycle is achieved from higher amplitude. The third force has the same amplitude, $P = 10^6$ Pa, but different spatial distribution: it mostly consists of the first mode only. Under this load, the plate starts to oscillate in the non-resonant limit cycle, making at least 16 oscillations. However, after that the limit cycle is switched to the resonant. This behaviour is explained by the fact that $M = 1.15$ is very close to M_{res} , and both limit cycles are close so that their basins of attraction are also close. Under such conditions, a relatively small disturbance (caused by the flow) of a limit cycle, which excites the second mode, can switch oscillations from one attractor to the other, which is shown in Fig. 19.

The same calculations conducted for a higher Mach number, $M = 1.27$, are shown in Fig. 20. The small-amplitude force contains both mode components, whereas the high-amplitude force excites only the first mode. At this M , the difference between resonant and non-resonant limit cycles is more pronounced, and switching the oscillations from one limit cycle to the other one needs more significant disturbance applied to the plate. Thus, the perturbation of the first mode caused by the flow, which forced such a switch at $M = 1.15$, is not large enough to do this at $M = 1.27$, and two stable coexisting limit cycles are clearly observed in Fig. 20. The spectra of both limit cycles are shown in Fig. 21. The spectrum of the non-resonant limit cycle contains only the first-mode frequency and the triple one; the contribution of other peaks is negligible. The spectrum of the resonant limit cycle also contains a significant doubled frequency component. Note that the first-mode frequency of the non-resonant limit cycle is slightly higher, whereas the maximum plate deflection is lower than that of the resonant limit cycle, exactly as was analytically shown by Vedenev (2013b).

6.5. Supersonic speeds: high-frequency limit cycle oscillations

For the value of Mach number $M = 1.33$, high-frequency limit cycles were observed (Fig. 22). This case is apparently a borderline between 1:2 resonant limit cycle and non-periodic oscillations described below. Initially, the development of the 1:2 resonant limit cycle occurs through the above-mentioned scenario (Fig. 22a). However, with time passing, high-frequency components appear (Fig. 22b). Initially they grow and have quasi-chaotic appearance, but with time they tend to a purely harmonic limit cycle (Fig. 22c). The shape of the oscillating plate has a mixture of the second and the fourth natural mode shapes.

The latter limit cycle oscillations occur during a long period, $t = 1.1 \dots 1.6$, making more than 200 oscillations. However, slowly deviations of the amplitude appear, and at $t \approx 1.7$ s, the plate motion suddenly switches to another limit cycle

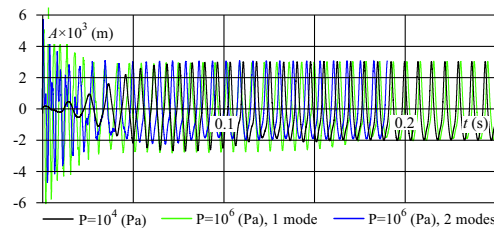


Fig. 19. Reference point deflection in time for different perturbation load, $M = 1.15$, $\mu = 1.64 \cdot 10^{-4}$.

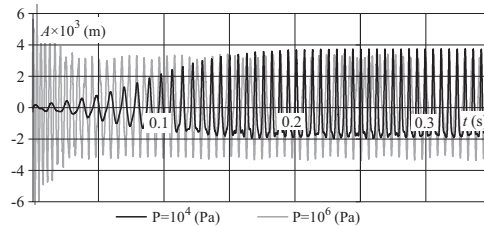


Fig. 20. Reference point deflection in time for different perturbation load, $M = 1.27$, $\mu = 1.64 \cdot 10^{-4}$.

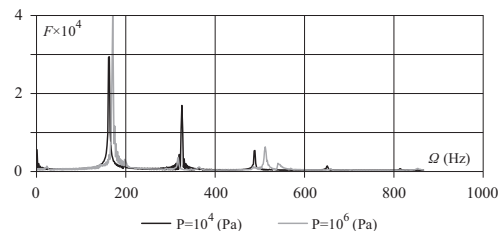


Fig. 21. Spectra of resonant and non-resonant limit cycles, $M = 1.27$, $\mu = 1.64 \cdot 10^{-4}$.

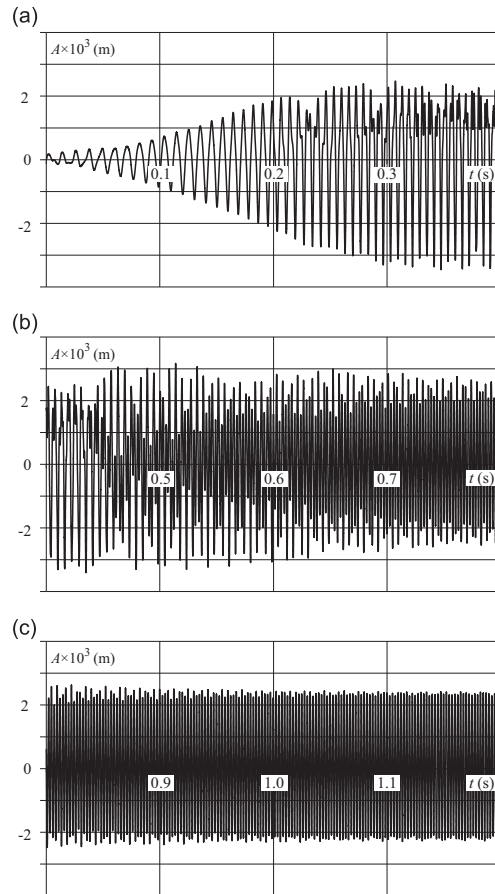


Fig. 22. Oscillation process and transition from low-frequency to high-frequency limit cycle for $M=1.33$. (a) Development of 1:2 resonant limit cycle, $t = 0 \dots 0.4$ s; (b) transition to high-frequency limit cycle, $t = 0.4 \dots 0.8$ s; (c) developed high-frequency limit cycle oscillations, $t = 0.8 \dots 1.2$ s.

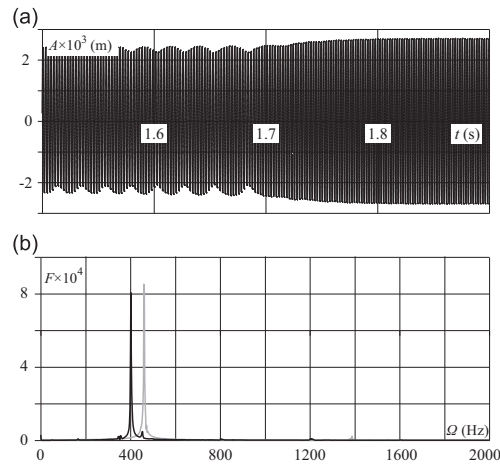


Fig. 23. Transition from one high-frequency limit cycle to another for $M=1.33$. (a) Reference point deflection, $t = 1.5 \dots 1.9$ s; (b) spectra for time ranges $t = 1.1 \dots 1.6$ (initially developed limit cycle, shown by black) and $t = 1.8 \dots 2.3$ (final limit cycle, shown by grey).

(Fig. 23a). The latter has higher amplitude and frequency (Fig. 23b), whereas the oscillation shape is a pure second natural mode shape (i.e., the fourth mode shape disappears). This limit cycle is apparently final for $M=1.33$, given that no other changes of the oscillation shape occur.

High-frequency limit cycles observed for $M=1.33$ obviously represent the development of linear instabilities of the second and the fourth modes found by Vedenev (2012, 2013a). Such limit cycles were also observed by Bendiksen and

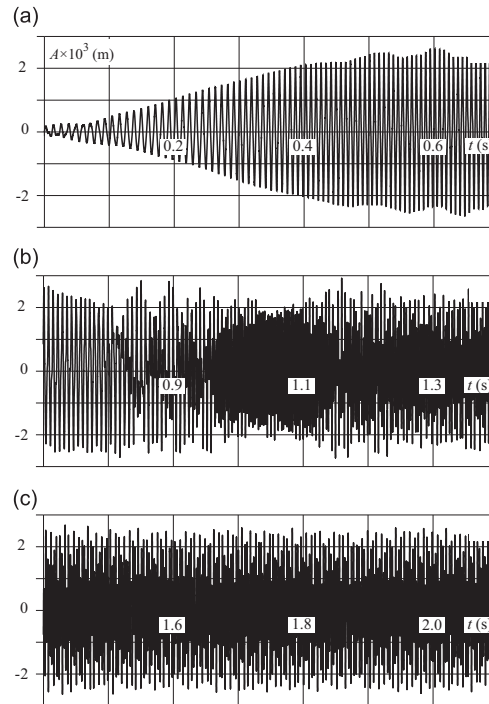


Fig. 24. Oscillation process and transition from limit cycle to chaotic-like high-frequency oscillations for $M=1.39$. (a) Development of a limit cycle, $t = 0 \dots 0.7$ s; (b) transition to high-frequency oscillations, $t = 0.7 \dots 1.4$ s; (c) developed high-frequency non-periodic oscillations, $t = 1.4 \dots 2.1$ s.

Davis (1995), Gordnier and Visbal (2002), and Alder (2015) for other flow conditions. Thus, high-frequency oscillations observed in the present study are in qualitative agreement with preceding works.

6.6. Supersonic speeds: non-periodic high-frequency oscillations

In the range of Mach numbers $1.36 \leq M < 1.42$, the oscillation process dramatically changes (Fig. 24). Initially the plate oscillates in the first mode. Thereafter, the second mode appears because of 1:2 resonance, as described above. However, slowly perturbations in the form of third, fourth, and fifth mode shapes appear. In contrast to the first and second modes, oscillations in higher modes are not periodic.

Because of the nonlinear mode interaction, oscillations in the first and second modes lose periodicity, and all the process becomes chaotic-like, without a dominant mode.

However, these oscillations are not ‘fully’ chaotic. Indeed, according to Schuster and Just (2005), there are several criteria that must be satisfied to consider the process as truly chaotic. These criteria are as follows:

1. Chaotic-like overall behaviour.
2. Positive maximal Lyapunov exponent.
3. Presence of wide-frequency bands in the spectrum.
4. Decrease of the autocorrelation function.
5. Poincaré section consists of points filling an open set of the space.

Consider these criteria in series. A close-up view of the resulting chaotic-like oscillations is shown in Fig. 25a; no periodicity of the reference point deflection is detected. Plate shapes captured at different moments of time are shown in Fig. 25b. There is no apparent regularity of the shapes: they include all mode shapes from the first to the seventh. The video of the oscillation process clearly shows a non-regular motion of the plate. Also, no periodicity is seen in the flow perturbation (Fig. 26).

However, additional calculations show that the second, third, and fourth criteria are not satisfied. We introduced a small perturbation of the plate during developed non-periodic oscillations and calculated the separation speed of the initial and perturbed trajectories in the phase space. This separation turned out to be linear, which means that the maximal Lyapunov exponent is not positive.

The spectrum of non-periodic oscillations, as shown in Fig. 25c, is essentially regular. It has several clear peaks, which means that the oscillations consist of several single-frequency components. However, in contrast to previous cases, their frequencies are not in a simple ratio. Namely, two dominating frequencies are $f_3 = 371$ and $f_4 = 603$ Hz, which is in 8:13

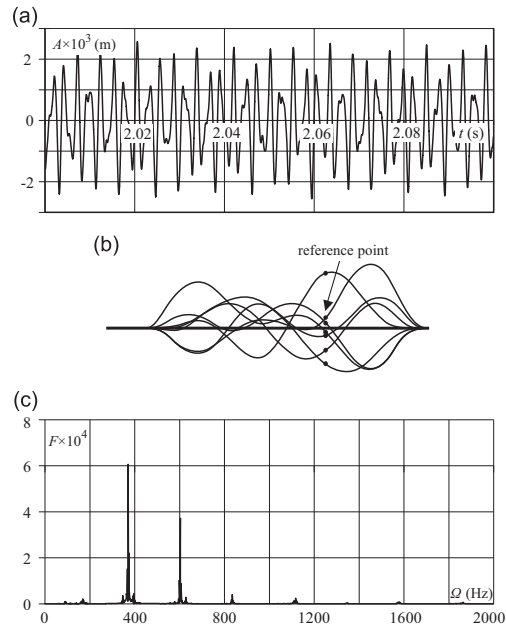


Fig. 25. Reference point deflection (close-up view of the Fig. 24) (a), plate shape (vertical scale 30:1) (b), oscillation spectrum (c). $M=1.39$.

ratio. This means that either the attractor has a significant 8:13 internal resonance component, or those frequencies are excited by the flow independently. Although lower peaks, $f_1 = 89$ and $f_2 = 168$, have much less amplitude, they are present and relate to the two dominating peaks at other ratios: $f_1:f_3 \approx 6:25$, $f_2:f_3 \approx 5:11$. Higher frequency peaks, $f_5 = 835$, $f_6 = 1117$, $f_7 = 1340$, $f_8 = 1573$, and $f_9 = 1863$ Hz, are the derivatives of the dominating ones caused by the cubic nonlinearity of the plate: $f_5 = 2f_4 - f_3$, $f_6 = 3f_3$, $f_7 = 2f_3 + f_4$, $f_8 = 2f_4 + f_3$, and $f_9 = 5f_3$.

The autocorrelation function calculated for the developed non-periodic oscillations regime turned out to be periodic, not decreasing function so that the oscillations cannot be considered as truly chaotic.

On the other hand, the last criterion is satisfied, i.e., the Poincaré section fills a full segment. This means that the attractor is not a 'pure' limit cycle, as could be thought from the Lyapunov exponent, spectral, and autocorrelation function criteria. But it is also not fully chaotic and is probably somewhat similar to irrational winding of a torus, which is a regular but non-periodic path on a torus, whose Poincaré section fills an open set.

As in the case of 1:2 resonant limit cycle, the change of the disturbing force can change the resulting oscillations. In that case, only two limit cycles were possible, and the switch from one to the other required significant change of disturbing force amplitude and spatial distribution. At higher M , when more modes are linearly growing, many more attractors can coexist, including limit cycles with higher internal resonances. In our calculations with different disturbing forces (either in amplitude or in spatial distribution) or slightly different flow speeds, we observed different non-periodic oscillations. They have similar displacement amplitudes of 2...3 plate thicknesses, but the spectra include additional frequency components that represent additional higher modes visible in instantaneous plate shapes.

6.7. Return to regularity and stability

When the Mach number is further increased, chaotic-like oscillations disappear. Surprisingly, in the range $1.42 \leq M \leq 1.67$, oscillations again occur in the form of a limit cycle. For $M=1.42$, it consists of two frequencies, 366 and 609 Hz, being in the 3:5 ratio, and the oscillations are purely periodic. For $M=1.44$ and 1.45, the limit cycle consists of two first natural modes; for higher M , it has the first natural mode only. For the latter case, the typical reference point deflection, plate shape, and spectrum are similar to those shown in Fig. 15. In other words, starting from $M=1.42$, attractors of the plate motion pass the same stages as before chaotic-like oscillations, but in the reverse order. When the Mach number increases, the limit cycle amplitude decreases and becomes almost zero for $M > 1.67$, which means return to stability of the flat state of the plate. This stability is maintained for higher M until the coupled-mode flutter occurs. For the dimensionless flow density $\mu = 1.64 \cdot 10^{-4}$ considered in this study, the coupled-mode flutter, according to (3), occurs for $M > M_{cr} = 2.92$.

6.8. Phase portraits

Consider phase portraits generated by motion of the reference point at different Mach numbers. For $M < 1.33$, when the attractor is a limit cycle, the phase portraits are shown in Fig. 27. At $M=1$ (Fig. 27a), when the limit cycle in fact consists of two diverged states changing each other, its shape in the phase space is condensed in the vertical direction. For higher M , while the

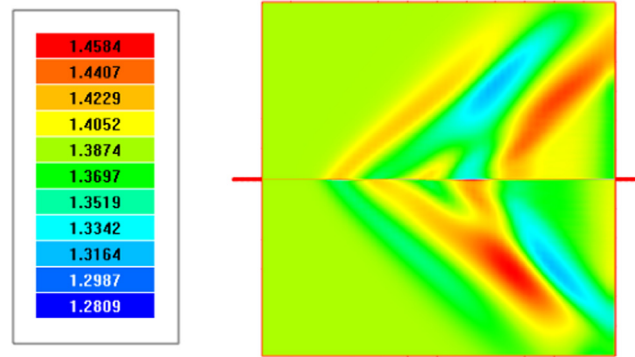


Fig. 26. Snapshot of the Mach number distribution at $M=1.39$.

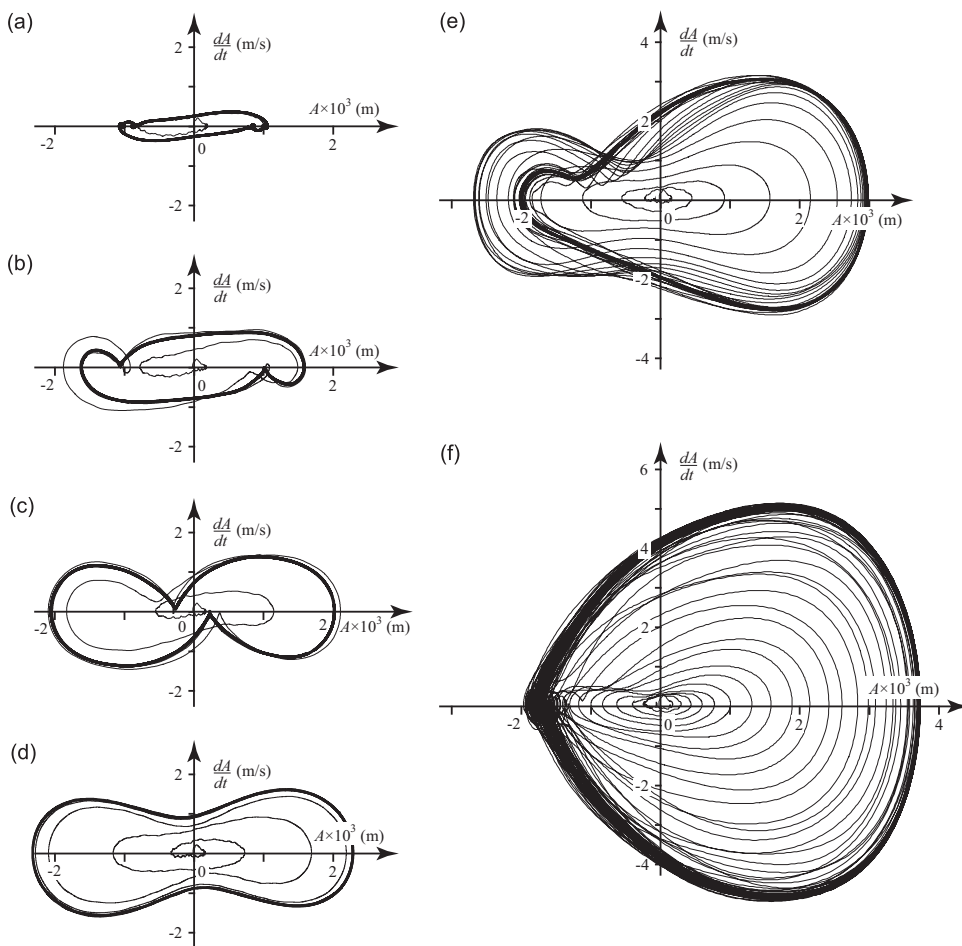


Fig. 27. Phase portraits of flutter oscillations. Non-resonant limit cycles: (a) $M=1.00$, (b) $M=1.03$, (c) $M=1.06$, (d) $M=1.09$; resonant limit cycles: (e) $M=1.15$, (f) $M=1.30$. Thin lines: evolution of the plate oscillations; bold lines: limit cycle oscillations. Axis scales in all figures are the same.

non-resonant limit cycle remains the only limit cycle (Fig. 27b–d), the limit cycle spreads in both horizontal and vertical directions, staying symmetric around the point $(0, 0)$. Note that the limit cycles are not elliptic (and, generally, not a Lissajous figure) because of triple-frequency harmonic present in the spectrum. For higher M (Fig. 27e–f), the resonant limit cycle appears, coexisting with the non-resonant one (not shown). The limit cycle becomes non-symmetric and spreads more significantly, especially along the vertical direction. The reason of this spread is the appearance of the second mode, whose doubled frequency yields increase of the plate velocities. During the initial evolution of the trajectory in Fig. 27e, the

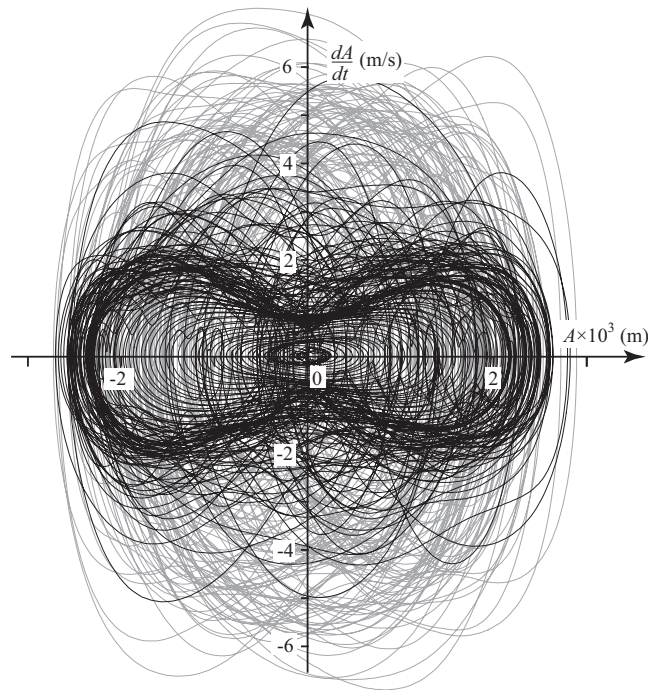


Fig. 28. Phase portraits of non-periodic flutter oscillations, $M=1.39$. Black curve: initial phase of evolution of the plate oscillations, $t=0\ldots 0.93$ s. Grey curve: development of chaotic-like oscillations, $t=0.93\ldots 1.25$ s.

appearance of the non-resonant limit cycle is observed. However, the growing resonating second mode yields the switch of the oscillations to the resonant limit cycle (Fig. 19).

The phase portrait of non-periodic oscillation at $M=1.39$ is shown in Fig. 28. The initial phase of the trajectory evolution is shown by the black curve; oscillations along the single-mode limit cycle are clearly observed during this phase. The second phase, development of non-periodic oscillations, is shown by the grey curve. The trajectory essentially spreads along the vertical direction because of the appearance of higher modes with higher frequencies, which yields increase of the plate velocities. It is seen that the trajectory does not follow any one-dimensional attractor.

6.9. Flutter amplitude

Fig. 29a shows the oscillation amplitudes (namely, amplitudes of the reference point). When the plate diverges, starting from $M \approx 0.76$, an increase of Mach number yields increase of the divergence amplitude. When passing through $M=1$, instability converts from divergence to flutter, which is accompanied by a slight drop of the amplitude. Next, when single-mode flutter occurs, the amplitude increases with increase of M even more rapidly than at divergence. Passing through the region of flutter with internal resonance yields split of the amplitude graph: plate oscillations are non-symmetric so that upper and lower graphs represent higher and lower amplitudes. For the same Mach numbers, single-mode limit cycle also exists, which means coexistence of two limit cycles. At $M \approx 1.3$, the maximum of amplitude is achieved: $A \approx 0.0039$ m. Further increase of Mach number is accompanied by the decrease of the amplitude, and by passing regions of high-frequency periodic and non-periodic oscillations. Beyond the latter, oscillation types are passed in the reversed order: high-frequency periodic oscillations, 1:2 resonant limit cycle, and first-mode limit cycle. The plate then returns to the stable state.

The important consequence from Fig. 29a is that the typical single-mode flutter amplitude is several times higher than that of the coupled-mode flutter (Fig. 9). This means that the single-mode flutter can cause fatigue damage much faster, and hence, it is more dangerous. The region of non-periodic oscillations is especially dangerous: even if the deflection amplitude is of the same order as for the first-mode limit cycle, the plate shape consists of higher natural mode shapes so that the stress amplitude is much higher than that of the first-mode limit cycle. On the other hand, higher modes have higher damping, which is an efficient way for single-mode flutter suppression, and the higher modes are likely to be totally damped. However, for long plates, natural structural damping is not always sufficient to overcome the linear growth (Vedeneev, 2013a) so that additional dampers may be necessary for the guaranteed flutter suppression.

Higher limit cycle amplitude at $M = 1.1\ldots 1.4$ than at larger M agrees with the results of Dowell (1974, p. 42) and Gordnier and Visbal (2002) obtained for different flow conditions.

The closed-form solution for the single-mode flutter amplitude (Vedeneev, 2007, 2013b) plotted in Fig. 29 shows the qualitative agreement between the numerical and analytical results. Two quantitative differences are observed: first, the oscillations occur at lower M , and second, their amplitude increases slower than the theory of Vedeneev (2013b) predicts.

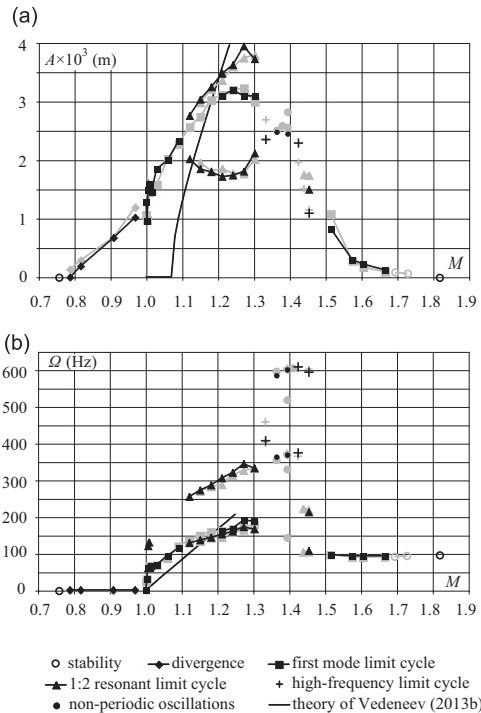


Fig. 29. Amplitudes of divergence and flutter (a); dominating frequencies (b) vs Mach number. Results for one-sided (black) and two-sided (grey) flow are shown.

The first difference is caused by the fact that in this study flutter occurs immediately at $M \geq 1$, whereas analytical theory (Vedeneev, 2013b) is not applicable to transonic flows and assumes that flutter occurs at a slightly higher M . The second difference is caused by different plate models (von Karman vs Mindlin plate theory), which yield different plate behaviours at amplitudes of the order of several plate thicknesses.

Fig. 29b shows the dominating frequencies of spectral peaks (except the triple frequency of the first one; it is caused by cubic plate nonlinearity and is not associated with a separate eigenmode). It is seen that the frequency growth in single-mode flutter region is almost linear. The frequency of the non-resonant limit cycle obtained in a closed form by Vedeneev (2013b), plotted in Fig. 29b, is qualitatively close to that obtained in the present study. When 1:2 internal resonance occurs, frequency growth slows down. After passing through the high-frequency and chaotic regions, the frequency and the amplitude decrease.

6.10. Role of aerodynamic nonlinearity

Comparison of flutter amplitudes and spectra for one- and two-sided flows in Fig. 29 shows acceptable quantitative agreement, except the narrow vicinity of $M=1$. The only difference between these models is the aerodynamic nonlinearity. The coincidence of results suggests that this nonlinearity actually plays no role, and the only mechanisms governing limit cycle oscillations are the linear aerodynamics generating eigenmode growth and the structural nonlinearity governing the interaction between the eigenmodes and forming a limit cycle.

Another argument against the aerodynamic nonlinearity is the qualitative agreement with the analytical theory of Vedeneev (2007, 2013b), where linear aerodynamics was used. In that study, the physical mechanisms of both non-resonant and resonant limit cycles were revealed, and the amplitude and frequency of single-mode limit cycle obtained in the present study, in general, fall within that prediction. Although the starting point of the non-resonant limit cycle is different (which is caused by aerodynamic nonlinearity at transonic flow), the appearance of the resonant limit cycle agrees well: $M_{res} \approx 1.13$ in this study versus $M=1.14$ in the theory of Vedeneev (2013b). High-frequency limit cycles are explained, again, by the linear growth of higher eigenmodes (Vedeneev, 2012, 2013a). Non-periodic high-frequency oscillations are the only plate behaviour not fully understood at this point. However, there is a small chance that the aerodynamic nonlinearity plays any role there. It seems more likely that multiple linearly growing eigenmodes compete with each other during the nonlinear growth phase, and no one can win and form the limit cycle because of very narrow basins of attraction, or just instability of their limit cycles.

Thus, we suggest that the complex plate dynamics observed in this study and partially by Bendiksen and Davis (1995), Gordnier and Visbal (2002), and Alder (2015) is caused by linear aerodynamics and structural nonlinearity so that aerodynamic nonlinearity is negligible at all flow conditions, except the transonic flow. This agrees with Gordnier and Visbal (2002) and Alder (2015) who reported insignificant discrepancy for $M=1.2$ between their Euler computations and potential flow (i.e., linearised Euler) study of Dowell (1974) both in flutter boundary and limit cycle amplitude. On the other hand, at $M=1.41$ they

observed a discrepancy with potential flow results, which was explained by the aerodynamic nonlinearity (Gordnier and Visbal, 2002). We note that the frequency of their limit cycle at $M=1.41$ is 3...5 times higher than at $M=1.2$ so that we suppose that at $M=1.41$ they observed a higher-mode limit cycle. Dowell (1974) has not reported any evidence of high-frequency limit cycles, that is why we suggest that the discrepancy between Euler and potential flow computations at $M=1.41$ is because of different limit cycles observed but not because of the aerodynamic nonlinearity.

Note that the flow conditions investigated in this study assume the dynamic pressure $200 < \lambda^* < 520$. It is possible that higher dynamic pressures yield more significant role of the aerodynamic nonlinearity, such as non-symmetric positive and negative divergence displacements obtained by Gordnier and Visbal (2002) and Alder (2015) for $M=0.95$, $\lambda^* > 800$.

7. Conclusions

Nonlinear development of divergence, single-mode, and coupled-mode flutter oscillations of a plate has been numerically studied. Amplitudes and frequencies of flutter oscillations have been obtained. In the case of high Mach numbers, excellent correlation with classical results based on piston theory has been achieved. In the case of low supersonic flow, four types of flutter oscillations have been observed: first-mode limit cycle, limit cycle that includes internal 1:2 resonance between the first and the second modes, high-frequency periodic oscillations, and high-frequency non-periodic plate oscillations.

While the first- and higher-mode limit cycles were observed in previous studies (Bendiksen and Davis, 1995; Gordnier and Visbal, 2002), flutter oscillations with internal resonance and non-periodic high-frequency oscillations are new findings in the present work. The results show that non-resonant and resonant limit cycles can coexist so that the final limit cycle depends on the initial perturbation, which is consistent with the theoretical study of Vedenev (2013b). For sufficiently small flow density, there is a gap of Mach numbers between single-mode ($1 < M < 1.67$) and coupled-mode (large M) flutter regions, where the plate is stable.

Comparison of flutter oscillations for the case of one- and two-sided flows suggests that in all cases, except the transonic flow, aerodynamic nonlinearity is insignificant so that flutter oscillations are driven by linear growth mechanism and structural nonlinearity of the plate.

The results show that the amplitude of flutter oscillations at low supersonic Mach numbers is typically several times higher than that of the coupled-mode flutter, as was predicted by Vedenev (2013b). Maximum stress amplitude is achieved at high-frequency oscillations and can be much higher than for other flutter types, which is caused by higher mode shapes dominating in the shape of the plate oscillations. This means that from the safety point of view, the single-mode panel flutter at low supersonic speeds can be much more dangerous than the classical coupled-mode flutter that occurs at higher speeds.

Acknowledgements

The work is supported by Russian Foundation for Basic Research (14-01-31547 and 14-01-00049) and grant MD-4544.2015.1.

References

- Aksenov, A.A., Dyadkin, A.A., Pokhilko, V.I., 1998. Overcoming of barrier between CAD and CFD by modified finite volume method. In: Proceedings of 1998 ASME Pressure Vessels and Piping Division Conference, San Diego, 377-2, pp. 79–86.
- Aksenov, A., Korenev, D., Shishaeva, A., Vucinic, D., Mravak, Z., 2008. Drop-Test FSI simulation with Abaqus and FlowVision based on the direct 2-way coupling approach. In: Proceedings of Abaqus Users' Conference, Newport, Rhode Island, pp. 611–624.
- Alder, M., 2015. Development and validation of a fluid–structure solver for transonic panel flutter. *AIAA Journal*, <http://dx.doi.org/10.2514/1.j054013>, in press.
- Bendiksen, O.O., Davis, G.A., 1995. Nonlinear Traveling Wave Flutter of Panels in Transonic Flow, AIAA Paper 95-1486.
- Bolotin, V.V., 1963. *Nonconservative Problems of the Theory of Elastic Stability*. Pergamon Press, Oxford.
- Dowell, E.H., 1974. *Aeroelasticity of Plates and Shells*. Noordhoff International Publishing, Leyden.
- Dugundji, J., 1966. Theoretical considerations of panel flutter at high supersonic Mach numbers. *AIAA Journal* 4 (7), 1257–1266.
- Gordnier, R.E., Visbal, M.R., 2002. Development of a three-dimensional viscous aeroelastic solver for nonlinear panel flutter. *Journal of Fluids and Structures* 16 (4), 497–527.
- Grigolyuk, E.I., Lamper, R.E., Shandarov, L.G., 1965. Flutter of plates and shells. *Itogi nauki. Mekhanika*. 1963, VINITI, Moscow, pp. 34–90 (in Russian).
- Hashimoto, A., Aoyama, T., Nakamura, Y., 2009. Effect of turbulent boundary layer on panel flutter. *AIAA Journal* 47 (12), 2785–2791.
- Mei, C., Abdel-Motagal, K., Chen, R.R., 1999. Review of nonlinear panel flutter at supersonic and hypersonic speeds. *Applied Mechanics Reviews* 10, 321–332.
- Movchan, A.A., 1957. On stability of a panel moving in a gas. *Prikladnaya Matematika i Mekhanika* 21 (2), 231–243. (in Russian); translated in NASA RE 11-22-58 W, 1959.
- Schuster, H.G., Just, W., 2005. *Deterministic Chaos: An Introduction*. Wiley-VCH, Weinheim.
- Vedenev, V.V., 2005. Flutter of a wide strip plate in a supersonic gas flow. *Fluid Dynamics* 5, 805–817.
- Vedenev, V.V., 2007. Nonlinear high-frequency flutter of a plate. *Fluid Dynamics* 5, 858–868.
- Vedenev, V.V., Guvernyuk, S.V., Zubkov, A.F., Kolotnikov, M.E., 2010. Experimental observation of single mode panel flutter in supersonic gas flow. *Journal of Fluids and Structures* 26, 764–779.
- Vedenev, V.V., 2012. Panel flutter at low supersonic speeds. *Journal of Fluids and Structures* 29, 79–96.
- Vedenev, V.V., 2013a. Effect of damping on flutter of simply supported and clamped panels at low supersonic speeds. *Journal of Fluids and Structures* 40, 366–372.
- Vedenev, V.V., 2013b. Limit oscillatory cycles in the single mode flutter of a plate. *Journal of Applied Mathematics and Mechanics* 77 (3), 257–267.